Linearized large signal modeling, analysis, and control design of phase-controlled series-parallel resonant converters using state feedback

Aboushady, Ahmed A.; Ahmed, Khaled H.; Finney, Stephen J.; Williams, Barry W.

Published in:
IEEE Transactions on Power Electronics

DOI:
10.1109/TPEL.2012.2231700

Publication date:
2013

Document Version
Author accepted manuscript

Linearized Large Signal Modeling, Analysis, and Control Design of Phase-Controlled Series-Parallel Resonant Converters using State Feedback

Ahmed A. Aboushady, *Student member, IEEE*, Khaled. H. Ahmed, *Senior member, IEEE*, Stephen. J. Finney, and Barry. W. Williams

***Abstract*— This paper proposes a linearized large signal state-space model for the fixed-frequency phase-controlled series-parallel resonant converter. The proposed model utilizes state feedback of the output filter inductor current to perform linearization. The model combines multiple-frequency and average state-space modeling techniques to generate an aggregate model with dc state variables that are relatively easier to control and slower than the fast resonant tank dynamics. The main objective of the linearized model is to provide a linear representation of the converter behaviour under large signal variation which is suitable for faster simulation and large signal estimation/calculation of the converter state variables. The model also provides insight into converter dynamics as well as a simplified reduced order transfer function for PI closed loop design. Experimental and simulation results from a detailed switched converter model are compared with the proposed state-space model output to verify its accuracy and robustness.**

***Index Terms*— Large signal, phase control, series-parallel resonant converter (SPRC), state feedback.**

NOMENCLATURE

v_s	DC link supply voltage (V)
v_{AB}	Inverter output voltage (V)
n	Transformer turns ratio
v_{AB}`	Inverter output voltage referred to transformer secondary = nv_{AB} (V)
r_{Ls}	Internal resistance of resonant tank inductor (Ω)
L_s	Resonant tank inductance (μH)
r_l	Parasitic resistance of transformer referred to secondary (Ω)
L_l	Leakage inductance of transformer referred to secondary (μH)
r_T	Total equivalent resistance (Ω)
L_T	Total equivalent inductance (μH)
C_s	Resonant tank series capacitance (μF)
C_p	Resonant tank parallel capacitance (μF)
r_{Lo}	Internal resistance of output filter inductor (Ω)
L_o	Output filter inductance (mH)
C_o	Output filter capacitance (μF)
ω_s	Resonant tank fundamental frequency (rad/s)
i_L	Resonant tank inductor current (A)
v_{Cs}	Resonant tank series capacitor voltage (V)
v_{Cp}	Resonant tank parallel capacitor voltage (V)
i_{Br}	Bridge rectifier input current (A)
v_{Br}	Bridge rectifier output voltage (V)
$\overline{v}_{Br}$	Average bridge rectifier output voltage (V)
i_{Lo}	Output filter inductor current (A)
v_o	Output voltage (V)
i_o	Output current (A)

Manuscript received January 31, 2012; revised April 20, 2012, July 22, 2012, and October 5, 2012; accepted November 26, 2012. Paper no. TPEL-2012-01-0102.

A. A. Aboushady, S. J. Finney, and B. W. Williams are with the Power Electronics, Drives and Energy Conversions Group, Institute of Energy and Environment, University of Strathclyde, Glasgow, G1 1XW, U.K. (e-mail: ahmed.aboushady@strath.ac.uk;stephen.finney@strath.ac.uk; barry.williams@strath.ac.uk).

K. H. Ahmed is with the Electrical Engineering Department, University of Aberdeen, Aberdeen, AB24 3UE U.K. (e-mail: khaled@ieee.org).

I. INTRODUCTION

DC/DC power converters are employed in a variety of applications, including power supplies for computers, office equipment, spacecraft power systems, laptop and telecommunications equipment, as well as dc motor drives. This is achieved using switched-mode PWM, or resonant-mode converters which allow control and regulation of the output voltage. Nowadays dc/dc converters are a common technology for renewable energy source grid integration [1,2], dc microgrids [3], HVDC systems [4], offshore oil and gas systems [5] in addition to interfacing energy storage elements such as batteries in UPS systems [6].

Dc/dc resonant converters are an alternative to hard-switched PWM converters in dc power supply applications. This is due to their soft switching characteristics; hence give the possibility of boosting the switching frequency and

reducing the transformer and filter size and weight. However, this is usually a design trade-off with the relatively high resonant peak voltages and currents.

Several types of resonant converters have been applied in dc power supply applications. Series resonant converters have poor no-load regulation, poor short circuit characteristics and need a larger output filter capacitor [7-9]. However its switching losses decrease with load decrease. They are suitable for high-output-voltage low-output-current converters [10-13]. Parallel resonant converters [14-16] have better no-load regulation and are naturally short circuit proof due to the resonant tank inductor. However, high circulating resonant tank current means higher switching losses and the converter is better suited to applications with a relatively narrow input voltage range. The combination series-parallel resonant converter (SPRC) combines advantages of both and eliminates their drawbacks. It can operate over a large input voltage range and a large load range (no load to full load) while maintaining high efficiency [17-20]. For this reason, this paper focuses on application of the SPRC in dc power supplies.

Various control techniques have been used to control resonant converters. These can be broadly classified into variable frequency and fixed-frequency approaches. Variable frequency techniques include average-current control, frequency control, capacitor voltage control, diode-conduction-angle control, and optimal trajectory control [20-22]. However, these variable frequency techniques present practical disadvantages, like a wide noise spectrum which make it difficult to control EMI, more complex filtering is needed, and poor utilization of magnetic components. Also, the frequency control range is limited if zero voltage switching (ZVS) of the converter is to be achieved. Operation below resonance means ZVS is lost and the inverter switches operate with turn on losses. This necessitates the use of fast recovery anti-parallel diodes to avoid diode recovery shoot-through within the same inverter leg. Operation above resonance is preferred where the SPRC operates with lagging power factor, hence ZVS. However, an increase in switching frequency above resonance results in a large non-linear reduction in converter voltage gain. Therefore, if frequency control is to be implemented, a narrow range of frequency control above resonance is necessary to achieve both ZVS and an acceptable voltage gain. Fixed frequency control above resonance such as phase shift control [23-25] overcomes the problems of variable frequency control and offers good control of the output voltage via controlling the phase-shift angle between the inverter legs; hence the effective inverter output voltage duty-cycle ratio. For the aforementioned reasons, this paper focuses on fixed frequency phase control of a SPRC.

Modeling of resonant converters is more complex than PWM converters. This is mainly due to the non-linear coupling of its ac and dc state variables. Various modeling techniques have been proposed in literature for the SPRC. Steady-state operation has been analyzed [18, 26-30], providing good insight into converter behavior and overall steady state gain. Small signal models for the SPRC use linearized state-space models around an equilibrium point to enable stability analysis and closed loop design [31]. The resulting closed loop design, although eliminating error in the output voltage, results in an unsatisfactory dynamic response. Small signal models include discrete time domain [32-34] and multiple frequency techniques [35-37]. A method based on discrete time domain modeling has been proposed for low order converters. It becomes cumbersome with higher order converters. The multiple frequencies method transforms ac signals into dc signals at multiple frequencies, thereby providing a theoretically high accuracy model [38]. Although small signal model is sufficient for analysis and closed loop design, it cannot be used to estimate converter state variables under large signal variations, which is possible if the converter is operating with a wide range input voltage or variable load. Large signal models based on a describing function method have also been proposed for SPRC analysis [39,40]. However, due to model non-linearity, non-linear controllers such as the sliding mode technique [41,42] and robust optimal control [43] were designed for SPRC control.

In this paper, a linearized large signal model for the SPRC is obtained using a state feedback scheme. The latter utilizes measurement of the output filter inductor current to perform model linearization. The model is useful for faster simulation as well as large signal estimation/calculation of converter ac and dc state variables, which can be used for converter sensorless control. In section two, the non-linear nature of resonant converters is explained. An aggregate SPRC large signal model is derived in section three. In section four, the state feedback scheme necessary for linearization is introduced. More analysis is performed on the linearized system model in section five. Finally, the accuracy and robustness of the model are assessed and validity by comparing experimental and MATLAB simulation results, using a detailed switching model of the phase-controlled SPRC.

II. NON-LINEAR NATURE OF DC/DC RESONANT CONVERTERS

Fig. 1 shows the circuit diagram for a typical SPRC. The bridge rectifier, together with the output LC filter, act as a non-linear load to the resonant tank circuit. This non-linearity is clarified in Fig.2. Hence, the converter large signal response cannot be modeled using linear approaches such as conventional average state-space models.

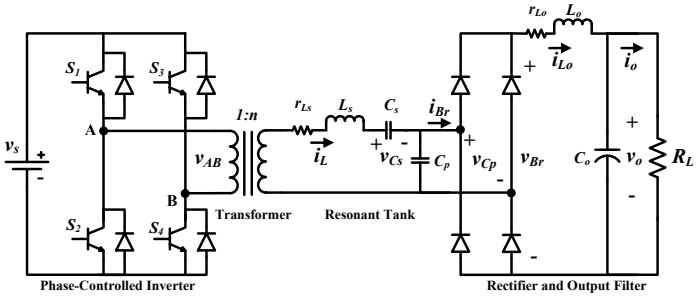

Fig. 1. Circuit diagram for the SPRC.

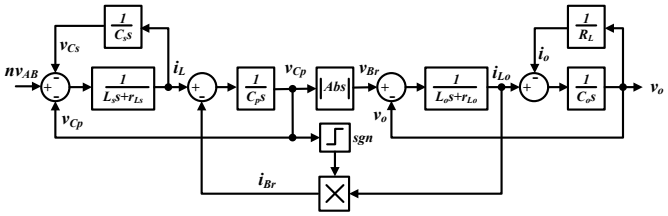

Fig. 2. Non-linear model representation of the SPRC.

III. PROPOSED MODEL FOR THE DC/DC RESONANT CONVERTER

Dc/dc resonant converters have two stages of conversion; dc/ac (inversion) and ac/dc (rectification). Hence, two main subsystems exist; the ac sub-system (resonant tank and transformer) and the dc sub-system (output filter), as illustrated in Fig. 3. Each sub-systems has its own state variables; therefore, both ac and dc state variables exist. In order to combine both types of signals into one model, it is essential to transform the ac state variables to equivalent dc quantities. This is achieved with the multiple frequency modeling (MFM) technique which converts the ac state variables to *d-q* quantities (dc values with slow dynamics) using an arbitrary synchronous reference frame. The resulting dc state variables from the resonant tank are combined with the natural dc state variables of the output filter side (modeled with conventional average state-space modeling) using a linearization scheme to overcome the non-linearity imposed by the rectifier. The result is an aggregate large signal linear model for the complete converter.

A. Ac sub-system modeling

Fig. 4 shows the equivalent circuit diagrams for the ac sub-system of the SPRC. Three state variables exist: i_L, v_{Cs}, v_{Cp}. The voltage-current relations are described by equations (1) to (3).

$$v_{AB}` = r_T i_L + L_T \frac{di_L}{dt} + v_{Cs} + v_{Cp} \tag{1}$$

$$i_L = C_s \frac{dv_{Cs}}{dt} \tag{2}$$

$$i_L - i_{Br} = C_p \frac{dv_{Cp}}{dt} \tag{3}$$

The multiple frequency modeling approach [35,36] for the SPRC, is utilized to model the ac sub-system of the resonant converter. Since the state variables have periodic characteristics, each state can be expressed by a Fourier series [37,38]. Energy transfers from the input to the output mainly at the fundamental frequency, hence the dominant frequency for modeling and analysis of the ac sub-system state variables is assumed to be ω_s , the operating frequency of the converter.

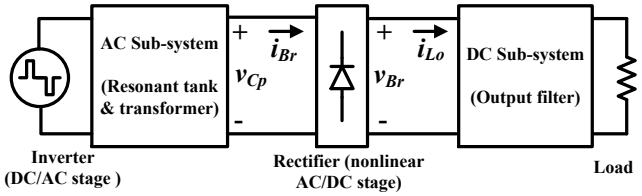

Fig. 3. Conversion stages and subsystems in a typical resonant converter.

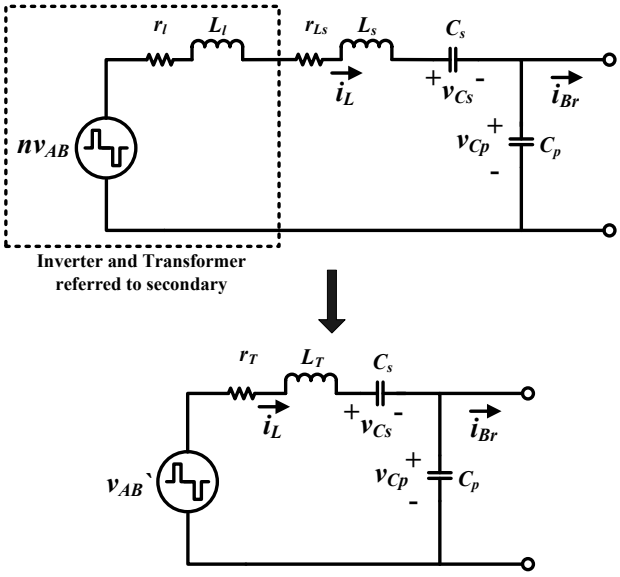

Fig. 4. Equivalent circuit diagrams for the AC sub-system.

The state variables and input can be approximated as sinusoidal states with fundamental frequency ω_s as in equations (4) to (8).

$$i_L = i_{Ld} \sin \omega_s t + i_{Lq} \cos \omega_s t \tag{4}$$

$$v_{Cs} = v_{Csd} \sin \omega_s t + v_{Csq} \cos \omega_s t \tag{5}$$

$$v_{Cp} = v_{Cpd} \sin \omega_s t + v_{Cpq} \cos \omega_s t \tag{6}$$

$$v_{AB}` = v_{ABd}` \sin \omega_s t + v_{ABq}` \cos \omega_s t \tag{7}$$

$$i_{Br} = i_{Brd} \sin \omega_s t + i_{Brq} \cos \omega_s t \tag{8}$$

where i_{Ldq}, v_{Csdq} and v_{Cpdq} are time-varying Fourier coefficients. These six Fourier coefficients, being time-dependent dc quantities, are considered as the new set of state variables. $v_{ABd}`$, $v_{ABq}`$, i_{Brd} and i_{Brq} are time-varying Fourier coefficients representing the new set of inputs to the model. Substituting equations (4)-(8) into equations (1)-(3), and equating sine and cosine coefficients, yields

$$v_{ABd}` = r_T i_{Ld} + L_T \frac{di_{Ld}}{dt} - L_T \omega_s i_{Lq} + v_{Csd} + v_{Cpd} \tag{9}$$

$$v_{ABq}` = r_T i_{Lq} + L_T \frac{di_{Lq}}{dt} + L_T \omega_s i_{Ld} + v_{Csq} + v_{Cpq} \tag{10}$$

$$i_{Ld} = C_s \frac{dv_{Csd}}{dt} - C_s \omega_s v_{Csq} \tag{11}$$

$$i_{Lq} = C_s \frac{dv_{Csq}}{dt} + C_s \omega_s v_{Csd} \tag{12}$$

$$i_{Ld} - i_{Brd} = C_p \frac{dv_{Cpd}}{dt} - C_p \omega_s v_{Cpq} \tag{13}$$

$$i_{Lq} - i_{Brq} = C_p \frac{dv_{Cpq}}{dt} + C_p \omega_s v_{Cpd} \tag{14}$$

Equations (9)-(14) in state-space form:

$$\dot{\vec{x}}_1(t) = A_1\vec{x}_1(t) + B_1\vec{u}(t) \tag{15}$$

where

$\vec{x}_1(t) = [i_{Ld}\ i_{Lq}\ v_{Csd}\ v_{Csq}\ v_{Cpd}\ v_{Cpq}]^T$, $\vec{u}_1(t) = [v_{ABd}`\ v_{ABq}`\ i_{Brd}\ i_{Brq}]^T$,

$$A_1 = \begin{bmatrix} -\frac{r_T}{L_T} & \omega_s & -\frac{1}{L_T} & 0 & -\frac{1}{L_T} & 0 \\ -\omega_s & -\frac{r_T}{L_T} & 0 & -\frac{1}{L_T} & 0 & -\frac{1}{L_T} \\ \frac{1}{C_s} & 0 & 0 & \omega_s & 0 & 0 \\ 0 & \frac{1}{C_s} & -\omega_s & 0 & 0 & 0 \\ \frac{1}{C_p} & 0 & 0 & 0 & 0 & \omega_s \\ 0 & \frac{1}{C_p} & 0 & 0 & -\omega_s & 0 \end{bmatrix} \quad B_1 = \begin{bmatrix} \frac{1}{L_T} & 0 & 0 & 0 \\ 0 & \frac{1}{L_T} & 0 & 0 \\ 0 & 0 & 0 & 0 \\ 0 & 0 & 0 & 0 \\ 0 & 0 & -\frac{1}{C_p} & 0 \\ 0 & 0 & 0 & -\frac{1}{C_p} \end{bmatrix}$$

B. Dc sub-system modeling

Fig. 5 shows the equivalent circuit diagram for the SPRC dc sub-system. Note that $\overline{v}_{Br}$ is the average rectifier output voltage v_{Br}. Energy is transferred at dc frequency, so the dominant component for modeling and analysis is the dc (average) value. For this reason, average state-space modeling, with a small-ripple assumption, is valid for modeling the dc sub-system.

Two state variables exist (i_{Lo} and v_o), for which the voltage-current relationships are described by (16) and (17). The bar notation denoting the average value of the state variables will be neglected for standardization of the model.

$$\overline{v}_{Br} = r_{Lo}i_{Lo} + L_o\frac{di_{Lo}}{dt} + v_o \tag{16}$$

$$i_{Lo} - i_o = C_o\frac{dv_o}{dt} \tag{17}$$

Equations (16) and (17) can be used to represent the dc sub-system in state-space form

$$\dot{\vec{x}}_2(t) = A_2\vec{x}_2(t) + B_2\vec{u}(t) \tag{18}$$

where

$\vec{x}_2(t) = [i_{Lo}\ v_o]^T$, $\vec{u}_2(t) = [v_{Br}\ i_o]^T$, $A_2 = \begin{bmatrix} -\frac{r_{Lo}}{L_o} & -\frac{1}{L_o} \\ \frac{1}{C_o} & 0 \end{bmatrix}$, $B_2 = \begin{bmatrix} \frac{1}{L_o} & 0 \\ 0 & -\frac{1}{C_o} \end{bmatrix}$

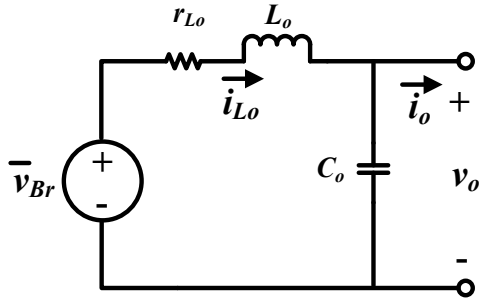

Fig. 5. Equivalent circuit diagram for the dc sub-system.

C. Combined system non-linear model

Fig.6 shows the non-linear model for the SPRC combining the state-space linear models of the ac and dc sub-systems. The voltage-current relationship between both sub-systems (separated by the bridge rectifier) is outlined by

- The state-variables of the ac sub-system are approximated as sinusoidal at the fundamental frequency, therefore

$$\overline{v}_{Br} = \frac{2}{\pi}v_{Br\_peak} = \frac{2}{\pi}v_{Cp\_peak} = \frac{2}{\pi}\sqrt{v_{Cpd}^2 + v_{Cpq}^2} \tag{19}$$

- Power balance theory: Output power from the ac sub-system is equal to input power to the dc sub-system (assuming lossless rectifier reverse recovery)

$$\frac{1}{2}\left(v_{Cpd}i_{Brd} + v_{Cpq}i_{Brq}\right) = \overline{v}_{Br}i_{Lo} \tag{20}$$

Substituting (19) into (20) yields

$$\frac{v_{Cpd}}{\sqrt{v_{Cpd}^2 + v_{Cpq}^2}}i_{Brd} + \frac{v_{Cpq}}{\sqrt{v_{Cpd}^2 + v_{Cpq}^2}}i_{Brq} = \frac{4}{\pi}i_{Lo} \tag{21}$$

As outlined by the analysis in [18], it can be also concluded that

$$i_{Br\_peak} = \frac{4}{\pi}i_{Lo} = \sqrt{i_{Brd}^2 + i_{Brq}^2} \tag{22}$$

Equations (21) and (22) confirm the non-linear relationship between the ac and dc sub-systems of the series-parallel resonant converter. Hence the voltage-current relationship can be represented by

$$\begin{aligned} i_{Brd} &= f\left(i_{Lo}, v_{Cpd}, v_{Cpq}\right) \\ i_{Brq} &= f\left(i_{Lo}, v_{Cpd}, v_{Cpq}\right) \end{aligned} \tag{23}$$

IV. State Feedback and Linearization

In this section, linear state feedback is used to linearize the relationship between the ac and dc sub-systems of the SPRC. The main objective of this linearization scheme is to formulate the necessary input voltages $v_{ABd}`$ and $v_{ABq}`$ to the resonant tank in Fig. 6 which force either outputs from the resonant tank (v_{Cpd} or v_{Cpq}) to be zero. In this case, the mathematical square-root relationship representing the diode rectifier reduces to a simple gain and both the ac and dc subsystems are cascaded linear systems that can be combined into one aggregate linear model. In order to realize this state feedback scheme, steady-state ac analysis of the resonant tank is performed to calculate the required input voltages $v_{ABd}`$ and $v_{ABq}`$. This is studied in the next sub-section and it is found that a measurement of the output filter inductor current is necessary to realise this linearization scheme.

A. Steady state analysis of ac sub-system

Fig.7 shows the steady state phasor diagram analysis for the ac sub-system (resonant tank), assuming sinusoidal state variables. The capital notation denotes steady state values. Starting with v_{Cp} and i_{Br} and working backwards (as from Fig. 4), the inverter voltage $v_{AB}`$ (referred to secondary) can be expressed as

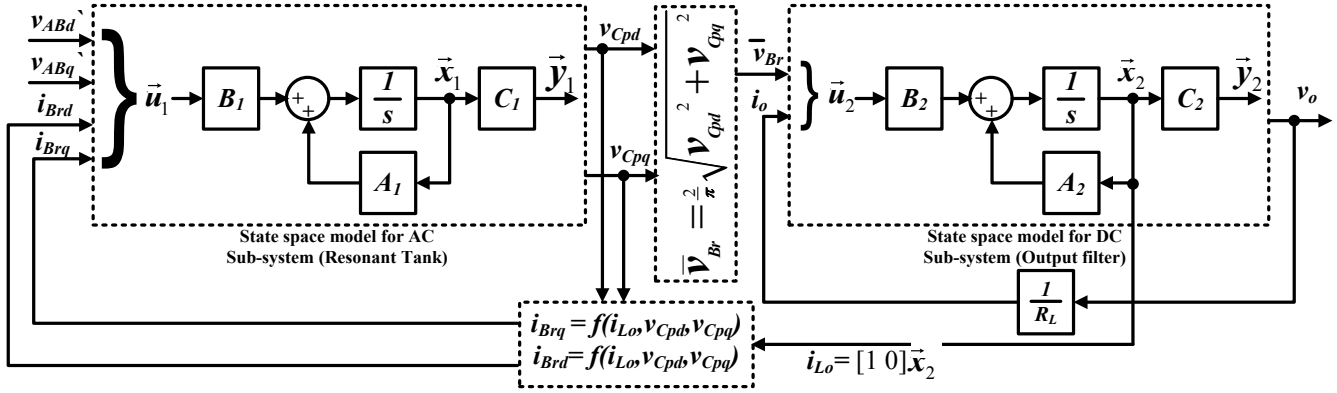

Fig. 6. Non-linear combined system model for the SPRC.

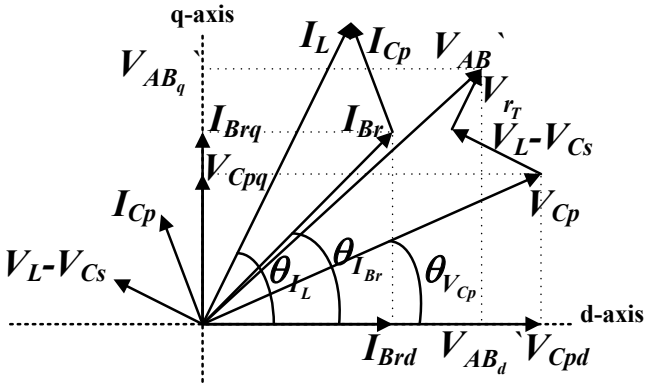

Fig. 7. Steady-state phasor diagram for the ac sub-system.

$$
\begin{aligned}
V_{ABd}` &= V_{Cp}\cos\theta_{V_{Cp}} + (V_L - V_{Cs})\cos(90+\theta_{I_L}) + V_{r_T}\cos\theta_{I_L} \\
&= V_{Cpd} + \left(\frac{1}{\omega_s C_s} - \omega_s L_T\right) I_L \sin\theta_{I_L} + r_T I_L \cos\theta_{I_L} \\
&= V_{Cpd} + \left(\frac{1}{\omega_s C_s} - \omega_s L_T\right)\left(I_{Brq} + I_{Cp}\cos\theta_{V_{Cp}}\right) + r_T\left(I_{Brd} + I_{Cp}\cos(90+\theta_{V_{Cp}})\right) \\
&= V_{Cpd} + \left(\frac{1}{\omega_s C_s} - \omega_s L_T\right)\left(I_{Brq} + V_{Cp}\omega_s C_p . \frac{V_{Cpd}}{V_{Cp}}\right) + r_T\left(I_{Brd} - V_{Cp}\omega_s C_p . \frac{V_{Cpq}}{V_{Cp}}\right) \\
&= V_{Cpd}\left(1 + \frac{C_p}{C_s} - \omega_s^2 L_T C_p\right) + V_{Cpq}\left(-r_T\omega_s C_p\right) + I_{Brd}\left(r_T\right) + I_{Brq}\left(\frac{1}{\omega_s C_s} - \omega_s L_T\right) \\
&= k_1 V_{Cpd} + k_2 V_{Cpq} + k_3 I_{Brd} + k_4 I_{Brq}
\end{aligned}
\tag{24}
$$

$$
\begin{aligned}
V_{ABq}` &= V_{Cp}\sin\theta_{V_{Cp}} + (V_L - V_{Cs})\sin(90+\theta_{I_L}) + V_{r_T}\sin\theta_{I_L} \\
&= V_{Cpq} - \left(\frac{1}{\omega_s C_s} - \omega_s L_T\right) I_L \cos\theta_{I_L} + r_T I_L \sin\theta_{I_L} \\
&= V_{Cpq} - \left(\frac{1}{\omega_s C_s} - \omega_s L_T\right)\left(I_{Brd} + I_{Cp}\sin\theta_{V_{Cp}}\right) + r_T\left(I_{Brq} + I_{Cp}\sin(90+\theta_{V_{Cp}})\right) \\
&= V_{Cpd} - \left(\frac{1}{\omega_s C_s} - \omega_s L_T\right)\left(I_{Brd} - V_{Cp}\omega_s C_p . \frac{V_{Cpq}}{V_{Cp}}\right) + r_T\left(I_{Brq} + V_{Cp}\omega_s C_p . \frac{V_{Cpd}}{V_{Cp}}\right) \\
&= V_{Cpd}\left(r_T\omega_s C_p\right) + V_{Cpq}\left(1 + \frac{C_p}{C_s} - \omega_s^2 L_T C_p\right) + I_{Brd}\left(\omega_s L_T - \frac{1}{\omega_s C_s}\right) + I_{Brq}\left(r_T\right) \\
&= k_5 V_{Cpd} + k_6 V_{Cpq} + k_7 I_{Brd} + k_8 I_{Brq}
\end{aligned}
\tag{25}
$$

where

$k_1 = k_6 = \left(1 + \frac{C_p}{C_s} - \omega_s^2 C_p L_T\right)$, $k_2 = -k_5 = -r_T\omega_s C_p$, $k_3 = k_8 = r_T$, and $k_4 = -k_7 = \left(\frac{1}{\omega_s C_s} - \omega_s L_T\right)$.

Expressions for the steady-state parallel capacitor voltage (V_{Cp}) can be obtained by solving (24) and (25) simultaneously and re-arranging

$$V_{Cpd} = \frac{k_6}{k_1 k_6 - k_2 k_5} V_{ABd}` - \frac{k_2}{k_1 k_6 - k_2 k_5} V_{ABq}` + \frac{k_2 k_7 - k_3 k_6}{k_1 k_6 - k_2 k_5} I_{Brd} + \frac{k_2 k_8 - k_4 k_6}{k_1 k_6 - k_2 k_5} I_{Brq} \tag{26}$$

$$V_{Cpq} = -\frac{k_5}{k_1 k_6 - k_2 k_5} V_{ABd}` + \frac{k_1}{k_1 k_6 - k_2 k_5} V_{ABq}` + \frac{k_3 k_5 - k_1 k_7}{k_1 k_6 - k_2 k_5} I_{Brd} + \frac{k_4 k_5 - k_1 k_8}{k_1 k_6 - k_2 k_5} I_{Brq} \tag{27}$$

Therefore, steady state values for the ac sub-system outputs (V_{Cpd} and V_{Cpq}) are obtained as a function of the inputs ($V_{ABd}`$, $V_{ABq}`$, I_{Brd} and I_{Brq}). This could be alternatively analyzed using state-space equation (15) at steady-state

$$0 = A_1 \vec{X}_1 + B_1 \vec{U} \tag{28}$$

$$
\begin{aligned}
\vec{X}_1 &= \begin{bmatrix} I_{Ld} & I_{Lq} & V_{Csd} & V_{Csq} & V_{Cpd} & V_{Cpq} \end{bmatrix}^T \\
&= -A_1^{-1} B_1 \begin{bmatrix} V_{ABd}` & V_{ABq}` & I_{Brd} & I_{Brq} \end{bmatrix}^T
\end{aligned}
\tag{29}
$$

B. State feedback scheme

The main objective of the linearization scheme is to calculate the necessary input voltages to the resonant tank $v_{ABd}`$ and $v_{ABq}`$ to force either outputs (v_{Cpd} or v_{Cpq}) to be zero, in order to circumvent the square-root non-linearity. Choosing either to be zero does not affect the modeling process as the objective is to control the converter output voltage. In this paper, v_{Cpq}=0. According to [18], the equivalent ac resistance at the rectifier input is given by

$$R_{ac} = \frac{V_{Cp}}{I_{Br}} = \frac{\pi^2}{8} R_L \tag{30}$$

This means that if v_{Cpq}=0, then it is also valid that i_{Brq}=0 due to the resistive relationship. According to (19)-(22), it also becomes true that $\bar{v}_{Br} = (2/\pi) v_{Cpd}$ and $i_{Brd}=(4/\pi) i_{Lo}$. Substituting V_{Cpq}=0 and I_{Brq}=0 into equations (26) and (27), and solving for $V_{ABd}`$ and $V_{ABq}`$ yields

$$V_{ABd}` = k_1 V_{Cpd} + k_3 I_{Brd} \tag{31}$$

$$V_{ABq}` = k_5 V_{Cpd} + k_7 I_{Brd} \tag{32}$$

Equations (31) and (32) show that the resonant circuit input voltage $V_{AB}`$ is a function of $I_{Brd}$ (proportional to the load current) and $V_{Cpd}$ (proportional to the output voltage). $V_{AB}`$ has to follow the relationship outlined by (31) and (32) in order to satisfy the main criteria for linearizing the converter model (I_{Brq}=0 and V_{Cpq}=0) and to ensure stable converter operation. The ac sub-system (resonant tank) is fed with

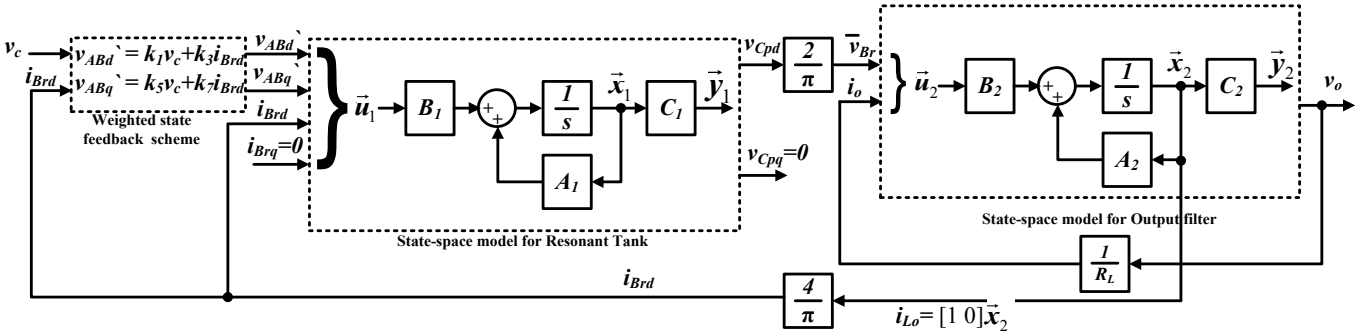

Fig. 8. Linearized model for the SPRC using weighted state feedback.

$$v_{ABd}` = k_1 v_c + k_3 i_{Brd} \tag{33}$$

$$v_{ABq}` = k_5 v_c + k_7 i_{Brd} \tag{34}$$

where v_c is a common control input for control of the converter output voltage. This scheme uses a weighted state feedback approach to linearize the resonant converter model. The weighted feedback is implemented using the output filter inductor current i_{Lo} as shown in Fig. 8.

C. Aggregate linear model

An aggregate model for the resonant converter can be obtained by combining the two linear state-space models in (15) and (18) for the ac and dc sub-systems respectively. Taking the relationship in (35) into account, yields the aggregate model in (36),

$$\begin{aligned} \bar{v}_{Br} &= \frac{2}{\pi} v_{Cpd},\ i_{Brd} = \frac{4}{\pi} i_{Lo},\ i_{Brq} = 0 \\ v_{ABd}` &= k_1 v_c + \frac{4}{\pi} k_3 i_{Lo} \\ v_{ABq}` &= k_5 v_c + \frac{4}{\pi} k_7 i_{Lo} \end{aligned} \tag{35}$$

$$\begin{aligned} \dot{\vec{x}}(t) &= A\vec{x}(t) + B\vec{u}(t) \\ y(t) &= C\vec{x}(t) \end{aligned} \tag{36}$$

where

$\vec{x}(t) = [i_{Ld}\ i_{Lq}\ v_{Csd}\ v_{Csq}\ v_{Cpd}\ v_{Cpq}\ i_{Lo}\ v_o]^T$, $\vec{u}(t) = [v_c\ \ i_o]^T$, $y(t) = v_o$,

$$A = \begin{bmatrix} -\frac{r_T}{L_T} & \omega_s & -\frac{1}{L_T} & 0 & -\frac{1}{L_T} & 0 & \frac{4k_3}{\pi L_T} & 0 \\ -\omega_s & -\frac{r_T}{L_T} & 0 & -\frac{1}{L_T} & 0 & -\frac{1}{L_T} & \frac{4k_7}{\pi L_T} & 0 \\ \frac{1}{C_s} & 0 & 0 & \omega_s & 0 & 0 & 0 & 0 \\ 0 & \frac{1}{C_s} & -\omega_s & 0 & 0 & 0 & 0 & 0 \\ \frac{1}{C_p} & 0 & 0 & 0 & 0 & \omega_s & -\frac{4}{\pi C_p} & 0 \\ 0 & \frac{1}{C_p} & 0 & 0 & -\omega_s & 0 & 0 & 0 \\ 0 & 0 & 0 & 0 & \frac{2}{\pi L_o} & 0 & -\frac{r_{Lo}}{L_o} & -\frac{1}{L_o} \\ 0 & 0 & 0 & 0 & 0 & 0 & \frac{1}{C_o} & 0 \end{bmatrix} \quad B = \begin{bmatrix} \frac{k_1}{L_T} & 0 \\ \frac{k_5}{L_T} & 0 \\ 0 & 0 \\ 0 & 0 \\ 0 & 0 \\ 0 & 0 \\ 0 & 0 \\ 0 & -\frac{1}{C_o} \end{bmatrix}$$

$$C = [0\ \ 0\ \ 0\ \ 0\ \ 0\ \ 0\ \ 0\ \ 1]$$

The aggregate linear model can also be represented using the transfer function technique

$$v_o(s) = \begin{bmatrix} G_1(s) & G_2(s) \end{bmatrix} \begin{bmatrix} v_c(s) \\ i_o(s) \end{bmatrix} \tag{37}$$

where

$G_1(s)$ is the control-to-output voltage transfer function

$$G_1(s) = \left.\frac{v_o(s)}{v_c(s)}\right|_{i_o=0} = C(sI_{8\times 8} - A)^{-1} B_{i1}$$

$G_2(s)$ is the output impedance

$$G_2(s) = \left.\frac{v_o(s)}{i_o(s)}\right|_{v_c=0} = C(sI_{8\times 8} - A)^{-1} B_{i2}$$

B_{ik} denotes row i column k of matrix B.

V. Linearized Converter Model Analysis

By considering the state-space model (36), Eigen values of the linearized system can be obtained by studying the complex s-plane. System Eigen values are obtained by (38), summarized in Table I, and plotted on the complex s-plane in Fig.9.

$$|sI_{8\times 8} - A| = 0 \tag{38}$$

Table I
Eigen Values for the Linearized Resonant Converter Model

Pole number	*Pole location in complex s-plane*	*Pole natural frequency, ω_n*
$P_{1,2}$	$\pm j\omega_s$	ω_s
$P_{3,4}$	$s_{p3,4}^{\ *}$	$\omega_{n_{p3,4}}^{\ *}$
$P_{5,6}$	$s_{p5,6}^{\ *}$	$\omega_{n_{p5,6}}^{\ *}$
$P_{7,8}$	$-\frac{r_{Lo}}{2L_o} \pm j\sqrt{\frac{1}{L_o C_o} - \frac{r_{Lo}^{\ 2}}{4L_o^{\ 2}}}$	$\frac{1}{\sqrt{L_o C_o}}$

* Defined in Appendix

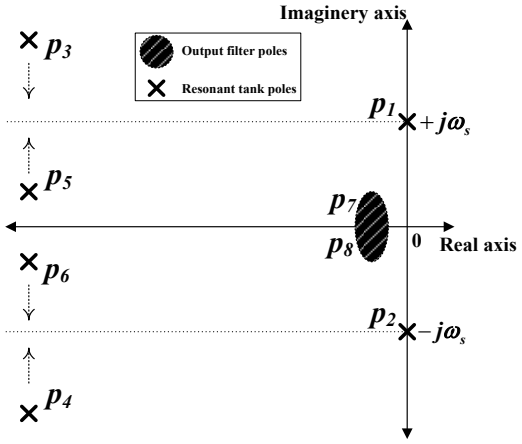

Fig. 9. Complex s-plane showing poles of the linearized resonant converter model.

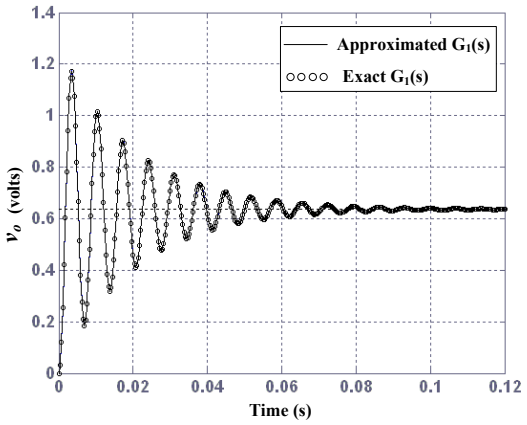

(b)

Fig. 10. Comparison between approximate and exact control-to-output voltage transfer function (a) Bode plots, and (b) step response.

B. Control-to-output voltage transfer function

By comparing the weighted state feedback scheme in (33)-(34) with (31)-(32), at steady-state v_{Cpd} is equal to the control input voltage v_c, i.e. $V_{Cpd}=V_c$. Then by examining Fig. 8, the control-to-output voltage transfer function $G_1(s)$ can be approximated by

$$G_1(s)=\frac{v_o(s)}{v_c(s)}\approx\frac{2}{\pi}\frac{v_o(s)}{\overline{v}_{Br}(s)} \tag{39}$$

This can be derived from state-space equation (18) of the dc sub-system (output filter)

$$G_1(s)\approx\frac{2}{\pi}\frac{1}{L_oC_os^2+r_{Lo}C_os+1} \tag{40}$$

Such a simplified second order control-to-output voltage transfer function is not to replace the derived model which provides detailed dynamics of the complete converter ac and dc state variables, but is useful for simplified closed loop PI control as in next subsection. In order to verify the validity of the approximated transfer function $G_1(s)$, Fig. 10 shows Bode plots and the step response comparing the behavior of the approximate control-to-output voltage transfer function with the exact transfer function $G_1(s)$ derived from (37).

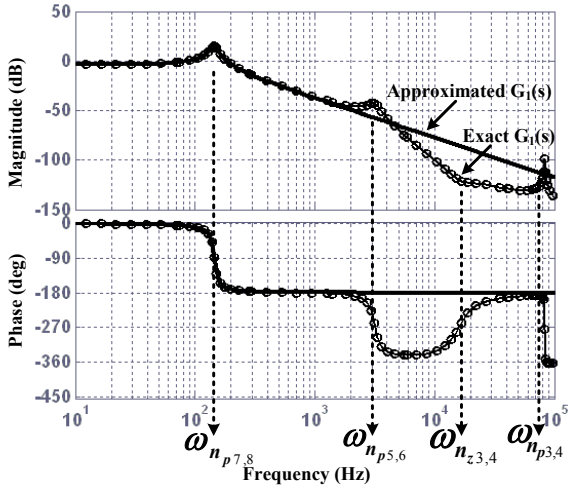

(a)

Fig. 10(a) shows that the second order low pass filter response of the approximate transfer function mimics the exact control-to-output voltage transfer function. The higher frequency dynamics (caused by poles $P_{3,4}$ and $P_{5,6}$) are attenuated by the output filter. The step response in Fig. 10(b) further proves the analogy in behavior of both the approximate and exact transfer functions. Such a reduced order transfer function is useful in simplifying the closed loop design procedure. Pole-zero placement can be readily applied.

C. Closed loop design

Since the dc/dc series-parallel resonant converter is used as a voltage source, the main objective is output voltage control. Hence, output voltage is used for feedback in a single control loop. No right-half plane zeros exist in the control-to-output voltage transfer function, so there is no need for a multi-loop structure [44]. PI control can be used, due to the aggregate model derived where all the state variables are dc. This means an infinite loop gain can be achieved by placing a pole at the origin, thereby eliminating steady state error in the output voltage [45]. Fig. 11 shows the closed loop structure to be used for PI control design. $C(s)$ is PI control in a pole-zero form with k_i as integral gain and k_p as proportional gain. The location effect of the real left-hand plane zero k_i/k_p is studied in Figs 12, 13 and 14 to select its best location for output response. The choice of k_p determines system overall stability. Fig. 12 shows root locus diagrams for different k_i/k_p. Since the zero of the PI controller is placed on the real-axis, it is moved in relation to the real part of the complex output filter pole-pair ($real(P_{7,8})=-r_{Lo}/2L_o$). The more k_i/k_p moves into the left hand plane, the more damped the closed loop poles for given k_p and oscillations are less effective.

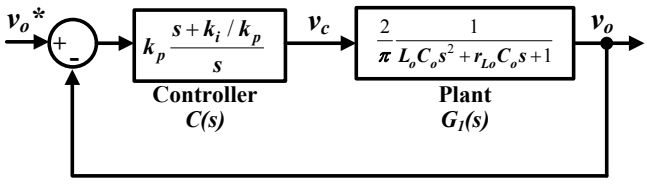

Fig. 11. Closed loop structure for output voltage control.

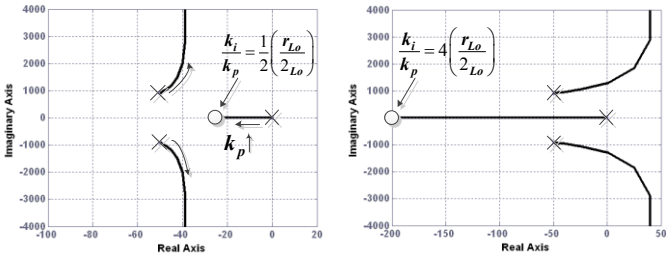

(a) (b)

Fig. 12. Root loci for the open loop transfer function $C(s)G_1(s)$

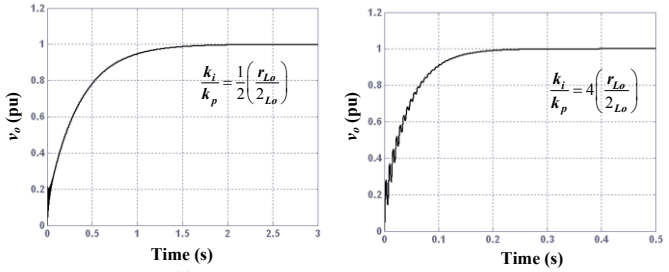

(a) (b)

Fig. 13. Closed loop step response for output voltage control loop

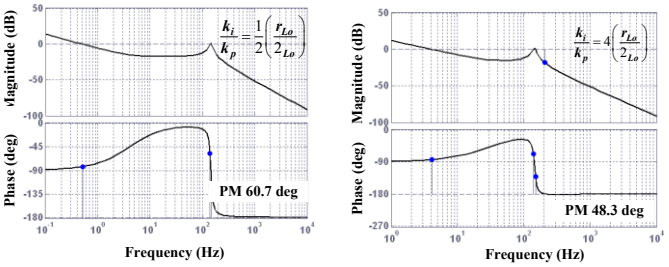

(a) (b)

Fig. 14. Open loop Bode plots

Although, for low values of k_i/k_p the closed loop stability margin is higher, however, system response is sluggish. Settling time cannot be reduced no matter how much k_p is increased. For this reason, high values of k_i/k_p are preferable for faster response though stability might be sacrificed due to a lower critical gain k_p for stability and lower phase margin. Fig. 13 shows the closed loop step response. Results confirm the slower rise and settling times with mitigated oscillations for higher k_i/k_p. The step response is mainly over-damped since it is dominated by the low frequency real closed loop pole. Its natural frequency is lower than that of the complex pole pair. This is clear from the under-damped step response in Fig.13(a) where k_i/k_p=0. Fig. 14 shows the open loop Bode plots with different controller zero locations. As described by the root locus analysis, stability margin (phase margin) is reduced as k_i/k_p is increased. Usually a phase margin of 45º to 60º is sufficient to ensure adequate closed loop stability. High dc loop gain is ensured with the origin pole (integrator) which provides zero steady state error for the output voltage; an essential characteristic for a voltage source.

D. Output impedance

Similar to the earlier analysis on the control-to-output voltage transfer function, the output impedance can be derived directly from the state-space model of the dc sub-system in (21). This is due to $V_{Cpd}=V_c$ at steady state. The output impedance transfer function $G_2(s)$ is

$$G_2(s)=\frac{v_o(s)}{i_o(s)}=-\frac{L_o s+r_{Lo}}{L_o C_o s^2+r_{Lo}C_o s+1} \quad (41)$$

The closed loop output impedance can be studied by examining Fig. 15(a) and is expressed by

$$\frac{v_o(s)}{i_o(s)}=\frac{G_2(s)}{1+C(s)G_1(s)}=-\frac{s(L_o s+r_{Lo})}{L_o C_o s^3+r_{Lo}C_o s^2+(1+\frac{2}{\pi}k_p)s+\frac{2}{\pi}k_i} \quad (42)$$

Fig.15(b) shows Bode plots for the open and closed loop output impedances. Any high frequency harmonic ripple in load current is attenuated by the converter output impedance. In dc/dc resonant converters, since the dominant frequency component of the load current is dc, open loop output impedance will result in a constant (voltage drop across r_{Lo}). This can be verified from the steady state gain in (41). For the closed loop, attenuation to the dc load current is achieved by the controller integrator, appearing as an origin-zero in (42). Higher k_i/k_p leads to greater attenuation and the closed loop has better disturbance rejection and robustness against load variations. Fig.15(c) shows the dynamic response of the closed loop voltage control to a step load change for different k_i/k_p.

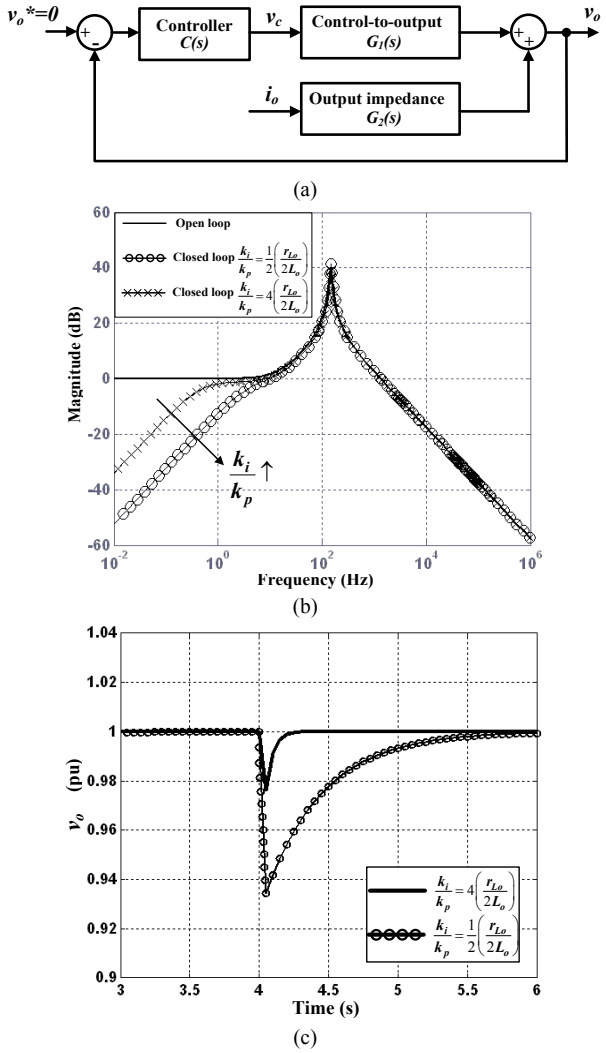

(a) (b) (c)

Fig. 15. (a) Control structure to obtain the closed loop output impedance, (b) Bode plots for open and closed loop converter output impedance, and (c) effect of changing k_i/k_p on closed loop response to a step load change.

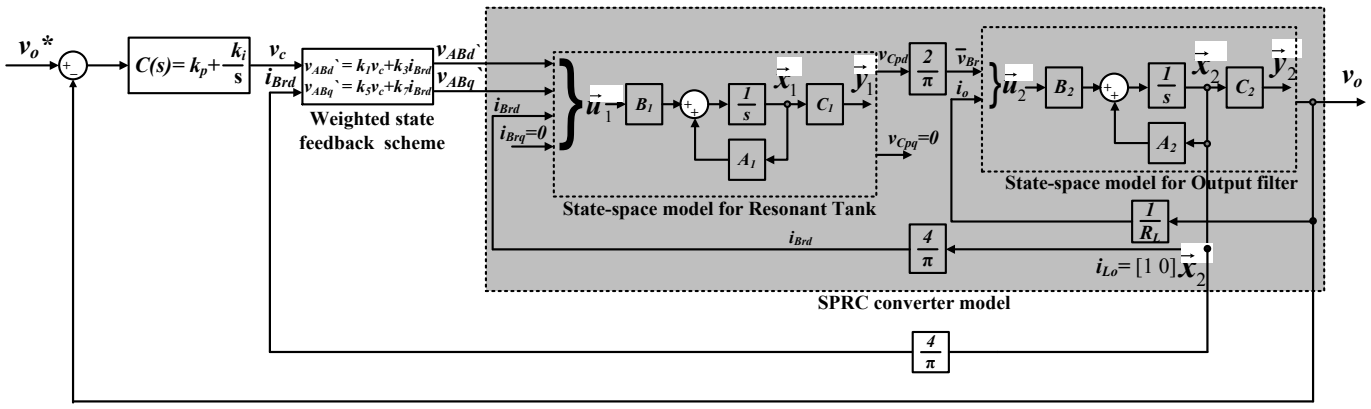

Fig. 16. Closed loop output voltage control of the SPRC using the proposed linearization scheme

VI. Simulation and Experimental Implementation

Fig. 16 illustrates the linearized SPRC closed loop output voltage control scheme, with the state feedback linearization scheme implemented. Closed loop voltage control of a 40W, 40 kHz phase-controlled SPRC is implemented experimentally and simulated in Matlab with a detailed switching model to verify the accuracy and robustness of the derived model in equation (37). Outputs from the derived model (the calculated/estimated state converter variables) are compared in Matlab with the detailed switching model of the converter and experimentally with actual converter measurements. Fig. 17 shows the control algorithm implementation both practically and in simulation and Table II summarizes the circuit and control parameter values.

Measurements of the actual SPRC output voltage (v_o) and output filter inductor current (i_{Lo}) are taken; the former to perform voltage control and the latter for state feedback linearization as shown in Fig17(a) and (b). Since i_{Lo} contains ripple due to the converter output filter, averaging is necessary since modeling of the dc subsystem (output filter) is based on an averaged state-space technique. Since the linearization scheme uses v_{Cpq}=0 and i_{Brq}=0, the i_{Brd} necessary for the linearization scheme is obtained from $i_{Brd}=(4/\pi)i_{Lo}$. The PI controller output v_c and $i_{Brd}=(4/\pi)i_{Lo}$ are inputs to the linearization scheme which calculates the necessary outputs v_{ABd}` &$v_{ABq}$` that force v_{Cpq}=0. The scheme is weighted by constants k_1, k_3, k_5 and k_7 which are based on the converter circuit parameters as defined by equation (25).

The phase shift angle δ between the inverter legs is then calculated by the algorithm in Fig. 17(c). With the state feedback outputs being v_{ABd}` &$v_{ABq}$` and knowing the supply voltage v_s and transformer turns ratio n, the phase-shift angle can be calculated. All the inverter switches are switched with a fixed 50% duty cycle; the only control variable being the phase shift angle between S_1 and S_3 as shown in Fig. 17(d). This controls the effective inverter output voltage duty cycle. The phase-shift angle is updated every switching cycle (25μs), viz., the inverter is switched at 40 kHz.

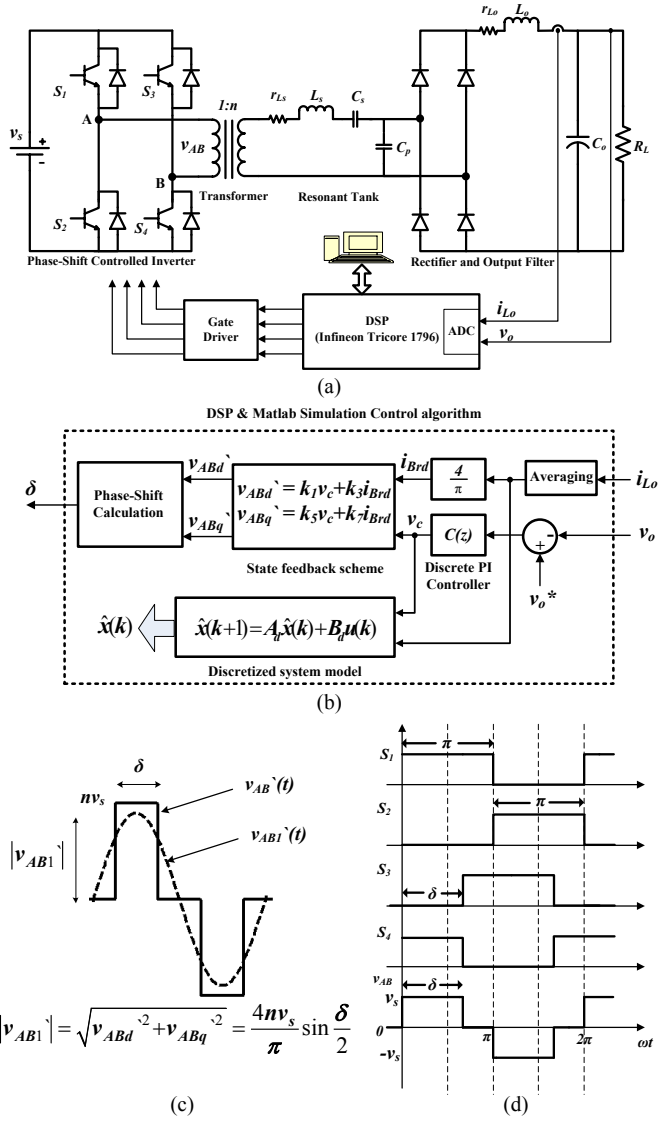

Fig. 17. Closed loop control algorithm with state feedback implemented: (a) circuit diagram, (b) control algorithm, (c) phase-shift calculator, and (d) inverter phase control gating pattern.

Table II
Resonant Converter Parameters

Parameter	*Value*
Internal resistance of resonant tank inductor r_{Ls}	0.1916 Ω
Resonant tank inductance L_s	100.13 µH
Parasitic transformer resistance referred to secondary r_l	0.6 Ω
Transformer Leakage inductance referred to secondary L_l	9.12 µH
Total equivalent resistance $r_T=r_l+r_{LS}$	0.7916 Ω
Total equivalent inductance $L_T=L_l+L_s$	109.25 µH
Resonant tank series capacitance C_s	0.255 µF
Resonant tank parallel capacitance C_p	0.255 µF
Internal resistance of output filter inductor r_{Lo}	0.5 Ω
Output filter inductance L_o	12.5 mH
Output filter capacitance C_o	120 µF
Resonant tank fundamental frequency f_s	40 kHz
Supply voltage v_s	60V
Transformer turns ratio n	0.5
Full-load power rating of experimental test rig	40W
Characteristic impedance of resonant tank $Z_c=\sqrt{L_T/C_s}$	20.7 Ω
Part-load resistive load R_{LPL}	40.5 Ω
Part-load Quality factor $Q_{PL}=Z_c/R_{LPL}$	0.511
Full-load resistive load R_{LFL}	14.4 Ω
Full-load Quality factor $Q_{FL}=Z_c/R_{LFL}$	1.44
PI controller parameters $(k_i/k_p)=5(r_{Lo}/2L_o)$	100 Hz
Proportional Gain k_p	0.1
Integral Gain k_i	10
Reference output voltage v_o^*	24V

In order to verify the linearized SPRC derived model, the state-space equation defining the system in (36) is discretized to estimate the converter state variables experimentally and in Matlab simulations. This allows the estimated results to be compared with measurements from the actual converter. The model is discretized with the main control algorithm interrupting at 25µs intervals, therefore, the sampling time used for discretization is T_s=25 µs. The discretized system is represented by

$$\hat{x}(k+1) = A_d\hat{x}(k) + B_d u(k) \tag{43}$$

where

$$A_d = e^{AT_S}$$

$$B_d = \int_0^{T_s} A(T_S - \boldsymbol{\tau})Bd\boldsymbol{\tau}$$

$$\hat{x}(k) = [i_{Ld}\ i_{Lq}\ v_{Csd}\ v_{Csq}\ v_{Cpd}\ v_{Cpq}\ i_{Lo}\ v_o]^T$$

$$u(k) = [v_c\ i_o]^T$$

i_o is the output (load) current which can be approximated by the average inductor current at steady state. Fig.18 shows the typical sampling diagram for the control algorithm implementation using an Infineon Tricore 1796 DSP with C-code execution times for the various control algorithm parts summarized in Table III.

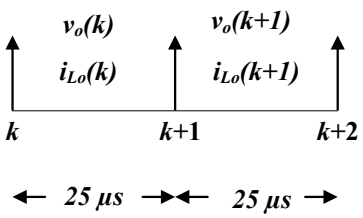

Fig.18 Sampling diagram

Table III
Program execution time for control algorithm

Task	*Execution time (µs)*
Fast ADC measurement	1
PI control loop	3
State feedback scheme	4
Phase shift calculation	2
State variables calculation/estimation	13
Total	23

A. Model accuracy study

The response of the linearized large signal model to large signal variations is studied in order to assess its ability to track real converter behavior. A step reference voltage from v_o^*=0 to v_o^*=24V is applied at t=0 and a step load change from part load (Q_{PL}=0.511) to full-load (Q_{FL}=1.44) is applied at t=5.0s. Simulation and experimental results are shown in Fig. 19 and 20 respectively. The experimental results illustrate actual converter measurements compared with calculated state variables using the derived model. The derived model uses equivalent dc quantities for the ac state variables of the resonant tank (i_L, v_{Cs} and v_{Cp}). These quantities (i_{Ld}, i_{Lq}, v_{Csd}, v_{Csq}, v_{Cpd} and v_{Cpq}) do not actually exist, therefore, results compare the actual converter ac state variables measured with the corresponding peak value of the state variable calculated using the model. The peak values are calculated from the model using

$$\begin{aligned} i_L &= \sqrt{i_{Ld}^2 + i_{Lq}^2} \\ v_{Cs} &= \sqrt{v_{Csd}^2 + v_{Csq}^2} \\ v_{Cp} &= \sqrt{v_{Cpd}^2 + v_{Cpq}^2} \end{aligned} \tag{44}$$

For display purposes on an oscilloscope, these estimated state variables are pulse width modulated and filtered to obtain their analogue peak values and are compared to the converter ac state variables measurements.

With the application of two large signal variations (step reference voltage at t=0 and step load at t=5.0s), the following can be deduced from Fig.19 and Fig. 20:

- The negligible differences between actual converter measurements and calculated state variables from the derived model verify the accuracy of the measured circuit parameters which the model depends on. Simulation and experimental results are closely matching.
- Calculated state variables track peak voltages and currents of the resonant tank as well as dc state variables of the output filter at steady state. However, slight variations occur in the transient response at the application of the large signal disturbance, especially in the voltage-based states v_o, v_{Cs} and v_{Cp} (Fig. 19(a), (d), (e) and Fig. 20(a), (c) and (d) respectively). This is because the model neglects, the ESR of the series-parallel resonant tank capacitors and the output filter capacitor. This is in order to avoid further model complication. Transient response of the current-based states such as i_L and i_{Lo} (Fig. 19(b) and (c) and Fig. 20(a) and (b) respectively) mimic the actual converter measurements.

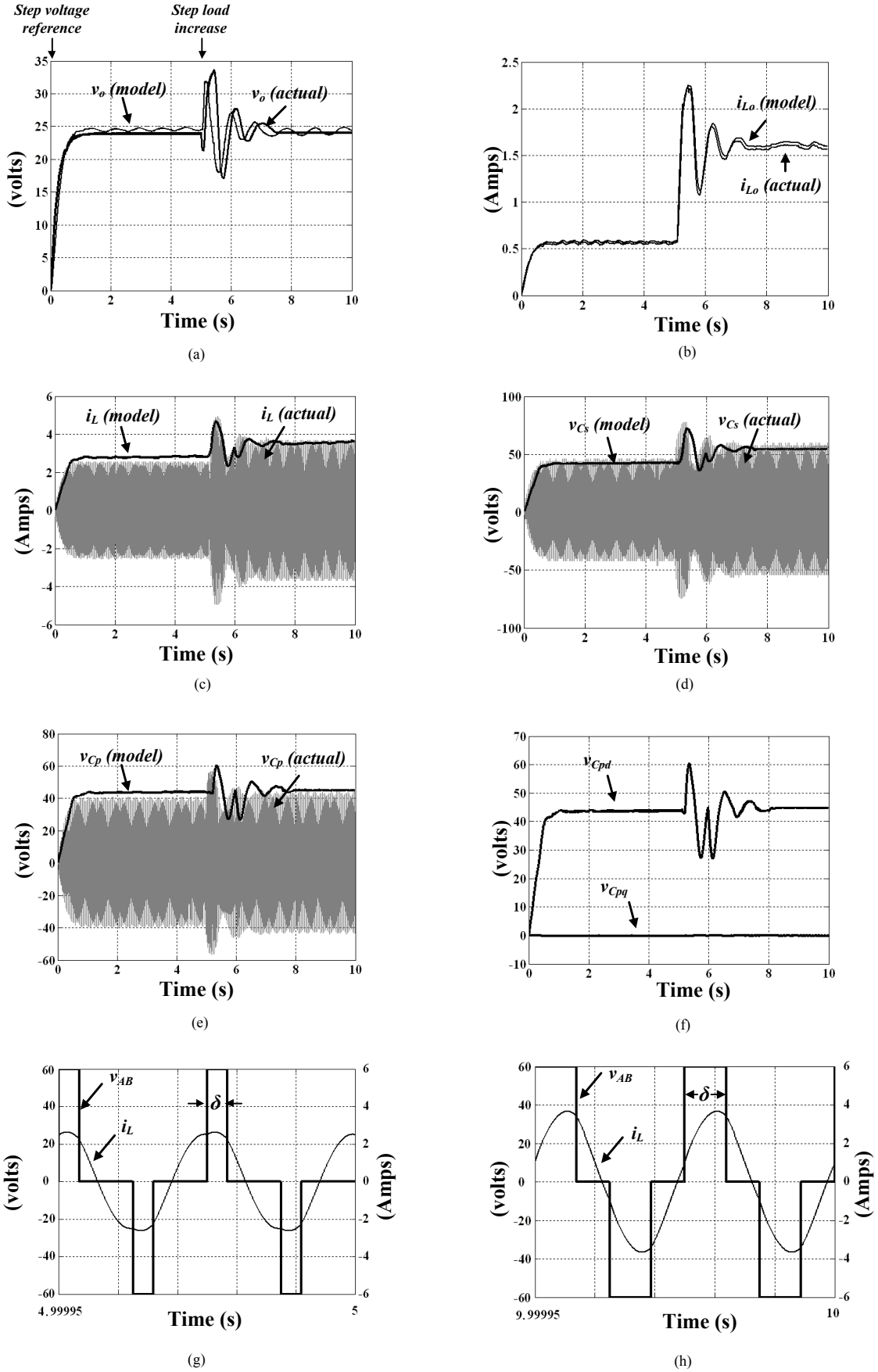

Fig. 19. Matlab simulations comparing actual switching and proposed large signal model (full-load applied at t=5.0s), (a) output voltage, (b) output filter inductor current, (c) resonant tank inductor current, (d) resonant tank series capacitor voltage, (e) resonant tank parallel capacitor voltage, (f) dq equivalent resonant tank parallel capacitor voltages, (g) inverter output voltage at part-load and (h) inverter output voltage at full-load

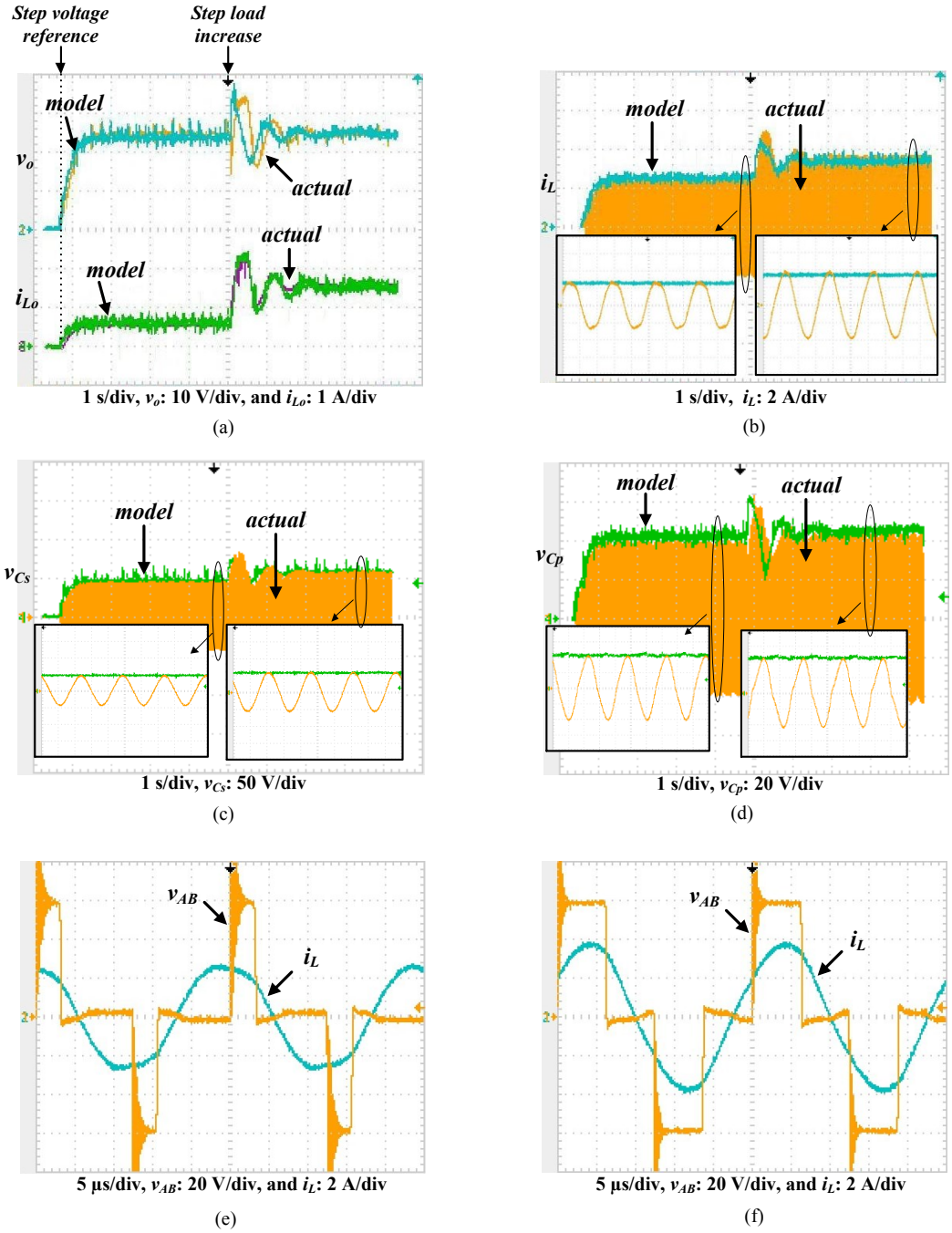

Fig. 20. Experimental results comparing measurements from the actual converter and the proposed large signal model, (a) output voltage and output filter inductor current, (b) resonant tank inductor current, (c) resonant tank series capacitor voltage, (d) resonant tank parallel capacitor voltage, (e) inverter output voltage at part-load (f) inverter output voltage at full-load

- Fig. 19(f) shows that the condition v_{Cpq}=0 outlined in (30)-(35) is maintained by the state feedback linearization scheme at all operating conditions. Also $v_{Cp(peak)} = v_{Cpd} \approx (\pi/2)v_o$. This verifies correct operation of the state feedback scheme.
- Fig. 19(g) and (h) and Fig. 20(e) and (f) show that after full load application (Q_{FL}=1.44), the control loop increases the phase shift angle δ to produce more fundamental voltage output from the inverter. This is inevitable as the converter voltage gain is reduced as Q increases, meaning more input voltage is required to maintain the required reference output voltage v_o^*=24V.
- Natural increases occur in the values of i_{Lo} and i_L after increased loading at t=5.0s. This causes an increased voltage drop on v_{Cs}, whereas the increase in v_{Cp} is marginal. The latter can be explained by the fact that v_{Cp} controls v_o, so it is fairly constant with a slight increase to compensate for the increased voltage drop on the output filter inductor parasitic resistance after the application of full load at t=5.0s.
- The PI controller disturbance rejection capability can be improved to reduce the transient effect at the load transition instant. This can be performed by increasing the k_i/k_p ratio but lower k_p gain would need to be used to avoid closed loop instability, which means a more sluggish response.

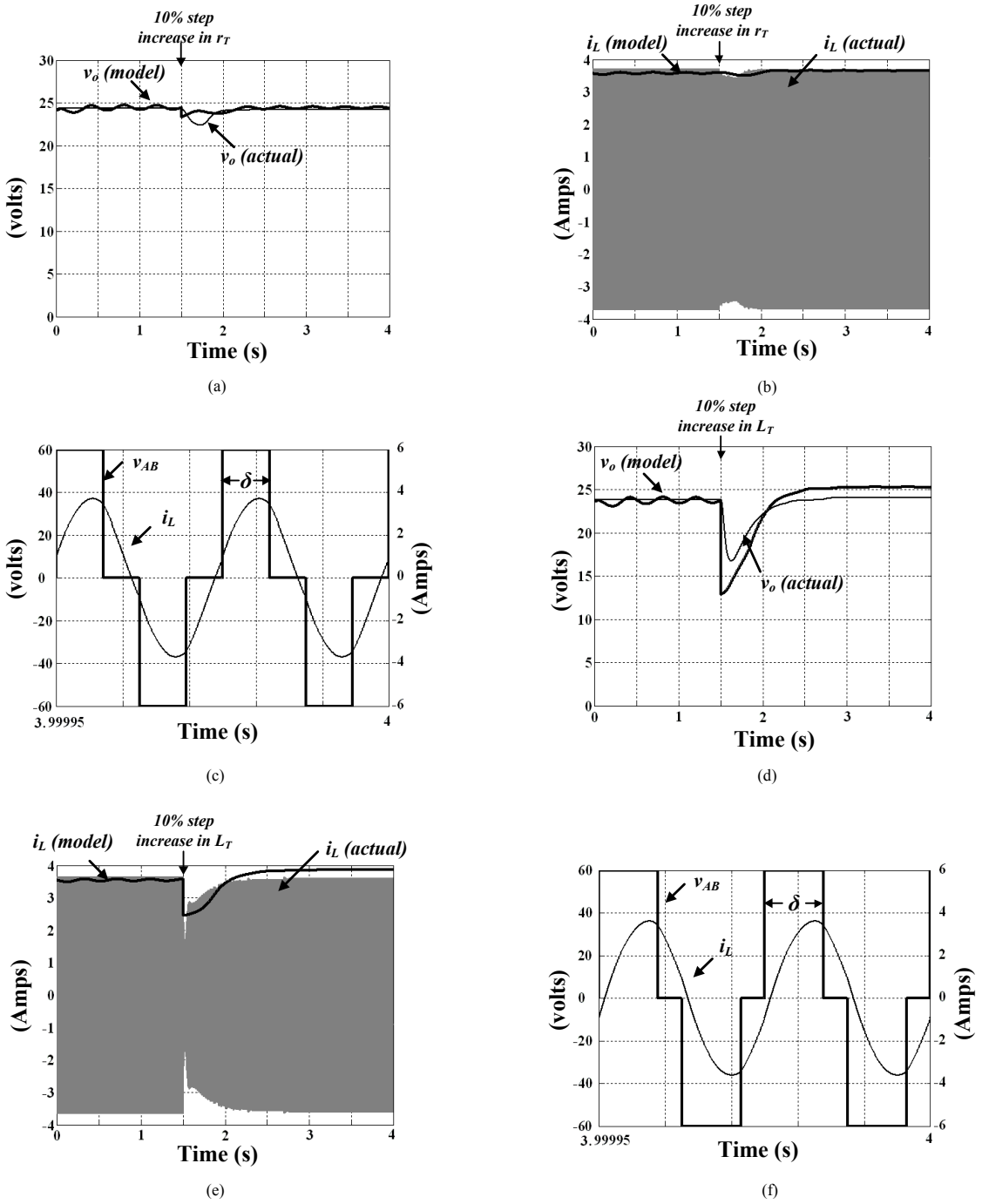

Fig. 21. Results for robustness analysis comparing the actual converter operating at full-load Q_{FL} with the proposed model, in response to a +10% step change (at t=1.5s) in the value of: (a)-(c) r_T and (d)-(f) L_T.

B. Model Robustness study

Circuit parameters practically vary during operation. Resistive elements are affected by temperature and transformers and/or magnetic-core inductors are affected by core saturation. In order to assess the robustness of the derived model against such variations, a 10% increase in selected circuit parameters is applied to the actual switched converter model in simulation and compared with the unchanged parameter's large signal model. Dominant circuit parameters that affect converter voltage gain are the resonant tank parasitic resistance r_T and equivalent inductance L_T which may be affected by changes in transformer leakage inductance. A 10% step increase in each parameter is applied to the converter operating at full load to assess the model's response. The new parameter values applied are r_T=0.87Ω and L_T=120μH. Closed loop results for each case are taken separately and illustrated in Fig. 21.

The effect of changing r_T is first studied. The actual converter's behavior has negligible change at steady-state since the results for v_o and i_L are virtually unchanged after t=1.5s, as shown in Fig.21(a) and (b) respectively. The proposed model is capable of tracking the changed system

parameter and estimates the state variables accurately. Fig. 21(c) confirms the minor effect on the converter due to changing r_T. This is shown by the analogous inverter output voltage v_{AB} and δ compared to the original case of converter operation with unchanged r_T as shown in Fig. 19(h).

The effect of changing L_T is shown in Fig. 21(d)-(f). The increase in L_T causes an increase in the resonant tank characteristic impedance. This causes a sudden drop in the output voltage v_o, and the control loop functions immediately in an attempt to correct this voltage sag by increasing the inverter output voltage via an increase of δ as shown in Fig.21 (f), when compared with Fig. 19 (h). The output voltage is restored to the reference value after about 1.5s due to the increased circuit time constant with increased L_T**.** However the model overestimates the output voltage by 5% due to the increased control input to the model. The resonant tank current i_L decreases slightly (as in Fig.21(e)) and similarly the model overestimates i_L by 6%. It can be concluded that the model is relatively insensitive to changes in the resonant tank parasitic resistance r_T whereas changing L_T has more of an effect on the model's performance. This is inevitable as the circuit resonant frequency changes and the entire dynamics of the converter are affected.

VII. Critical Evaluation

The original large signal non-linear model is an exact and precise representation of the converter for the whole load operating range. However, its non-linearity limits the application of simple and well known linear analysis and control techniques. Small signal models are an important linearization tool and have proven to be very successful for control design and stability analysis of many systems in the past. However the validity of the model remains limited in close neighbourhood of the steady state operating point and the model is not a true representative of large operational variations. From this perspective, the linearization scheme for the large signal model was proposed to preserve the large signal characteristics of the converter without linearizing around specific operating points. The methodology implemented for linearization can be merely viewed as an orientation of the ac subsystem dq state variables into an arbitrary reference frame to remove the main source of non-linearity; the mathematical "square root" function.

The proposed model has shown to provide closely matching results with the actual converter switched model. However, at high converter loading (high Q factor), the harmonic content in the resonant tank increases and the sinusoidal nature approximation of the resonant tank state variables becomes less accurate. This is mainly because a high Q factor means low load impedance compared to the resonant tank characteristic impedance. Consequently, the ratio of the injected square wave current from the bridge rectifier to the resonant circuit current is high, hence introducing higher order harmonics. Distortion introduced at high Q causes the proposed linearized model to have a marginal error in the value of the calculated state variables. This can be improved by assuming that resonant tank state variables are a harmonic series (instead of simply the fundamental component). However, this would result in n-times the existing number of resonant tank state variables, where n is the number of higher order harmonics included in the model. This makes the analysis way more difficult, tedious and increases the computation burden on the DSP and in return marginal improvement is achieved.

VIII. Conclusion

This paper proposes a feedback scheme that employs the output filter inductor current to obtain a linearized large signal model for the fixed-frequency phase-controlled SPRC. All state variables are converted to slow changing dc quantities which are easier to control than the fast resonant tank dynamics. The proposed state-space model represents converter behavior in response to large signal variations, and hence is useful for faster simulation in addition to estimating converter state variables for potential sensorless control applications. A reduced order transfer function was obtained to simplify the closed loop PI control design. PI control is sufficient to produce good closed loop dynamics and steady state performance. However, the limitation to increasing the proportional gain is the stability of the resonant tank. This can be improved by using multi-loop control. The model proved high accuracy when compared to the actual switching converter, and robustness against circuit parameter operational variation, especially changes in the resonant tank parasitic resistance. However, it is more sensitive to changes in the resonant tank inductance which is expected since the characteristic impedance and resonant frequency determining circuit behavior change accordingly.

Appendix

Parameters for Table II:

$$S_{p_{3,4}} = -\frac{r_T}{2L_T} \pm j\sqrt{\frac{-r_T^{\,2}C_sC_p + 4L_TC_s + 4L_TC_p + 4L_T^{\,2}C_sC_p\omega_s^{\,2} + 4L_T\omega_s\sqrt{4L_TC_sC_p^{\,2} + 4L_TC_pC_s^{\,2} - r_T^{\,2}C_s^{\,2}C_p^{\,2}}}{4L_T^{\,2}C_sC_p}}$$

$$s_{p_{5,6}} = -\frac{r_T}{2L_T} \pm j\sqrt{\frac{-r_T{}^2C_sC_p + 4L_TC_s + 4L_TC_p + 4L_T{}^2C_sC_p\omega_s{}^2 - 4L_T\omega_s\sqrt{4L_TC_sC_p{}^2 + 4L_TC_pC_s{}^2 - r_T{}^2C_s{}^2C_p{}^2}}{4L_T{}^2C_sC_p}}$$

$$\omega_{n_{p3,4}} = \sqrt{\frac{C_s + C_p + 4L_TC_p + L_TC_sC_p\omega_s{}^2 + \omega_s\sqrt{4L_TC_sC_p{}^2 + 4L_TC_pC_s{}^2 - r_T{}^2C_s{}^2C_p{}^2}}{L_TC_sC_p}}$$

$$\omega_{n_{p5,6}} = \sqrt{\frac{C_s + C_p + 4L_TC_p + L_TC_sC_p\omega_s{}^2 - \omega_s\sqrt{4L_TC_sC_p{}^2 + 4L_TC_pC_s{}^2 - r_T{}^2C_s{}^2C_p{}^2}}{L_TC_sC_p}}$$

REFERENCES

[1] N. Denniston, A.M. Massoud, S. Ahmed and P.N. Enjeti, "Multiple-module high-gain high-voltage dc-dc transformers for offshore wind energy systems", *IEEE Trans. on industrial electronics*, Vol. 58, No. 5, pp. 1877-1886, May 2011.

[2] Y.Y. Xia, J.E. Fletcher, K.H. Ahmed, S.J. Finney and B.W. Williams, "Torque ripple analysis and reduction for wind energy conversion systems using uncontrolled rectifier and boost converter", *IET Renewable Power Generation*, Vol. 5, Issue 5, pp. 377-386, 2011.

[3] A. Kwasinski, "Quantitative Evaluation of DC Microgrids availability: effects of system architecture and converter topology design choices", *IEEE Trans. on power electronics*, Vol. 26, No. 3, pp. 835-851, March 2011.

[4] L. Xu and L. Yao, "DC voltage control and power dispatch of a multi-terminal HVDC system for integrating large offshore windfarms", *IET Renewable Power Generation*, Vol. 5, Issue 3, pp. 223-233, 2011.

[5] T. Ericsen, N. Hingorani, and Y. Khersonsky, "Power electronics and future marine electrical systems," *IEEE Transactions on Industry Applications,* Vol. 42, No. 1, pp. 155-163, Feb 2006.

[6] K. Sun, L. Zhang, Y. Xing, J. M. Guerrero, "A Distributed Control Strategy Based on DC Bus Signaling for Modular Photovoltaic Generation Systems With Battery Energy Storage", *IEEE Trans. on Power Electronics*, Vol. 26, No. 10, pp. 3032-3045, October 2011.

[7] Y-K. Lo, C-Y. Lin, M-T. Hsieh and C-Y. Lin, "Phase-Shifted Full-Bridge Series Resonant DC-DC converters for Wide Load Variations", *IEEE Trans. on Industrial Electronics*, Vol. 58, No. 6, pp. 2572-2575, June 2011.

[8] M.S. Almardy and A.K.S. Bhat, "Three-phase (LC)-(L)-type series-resonant converter with capacitive output filter", *IEEE Trans. on Power Electronics*, Vol. 26, No.4, pp. 1172-1183, April 2011.

[9] B.R. Lin and S.F. Wu, "Implementation of a series resonant converter with series-parallel transformers", *IET Power Electron.*, Vol. 4, Issue 8, pp. 919-926, 2011

[10] H. Krishnasmawi and N. Mohan, "Three-port series-resonant DC-DC converter to interface renewable energy sources with bi-directional load and energy storage ports", *IEEE Trans. on Power Electronics*, Vol. 24, No. 10, pp. 2289-2297, October 2009.

[11] M. Castilla, L. Garcia de Vicuna, J. Matas, J. Miret and J. C. Vasquez, "A comparative study of sliding-mode control schemes for quantum series resonant inverters," *IEEE Trans. on Industrial Electronics*, Vol. 56, No. 9, pp. 3487-3495, Sept 2009.

[12] X. Li and A.K.S. Bhat, "Analysis and design of high frequency isolated dual-bridge series-resonant DC/DC converter", *IEEE Trans. on Power Electronics*, Vol. 25, No.4, pp. 850-862, April 2010.

[13] Y-C. Chuang, Y-L. Ke, H-S. Chuang and H-K.Chen, "Implementation and analysis of an improved series-loaded resonant DC-DC converter operating above resonance for battery chargers," *IEEE Trans. on Industry Applications*, Vol. 45, No.3, pp. 1052-1059, June 2009.

[14] H. Sheng, W. Shen, H. Wang, D. Fu, Y. Pei, X. Yang, F. Wang, D. Boroyevich, F.C. Lee and C.W. Tipton, "Design and implementation of a high power density three-level parallel resonant converter for capacitor charging pulsed-power supply", *IEEE Trans. on Plasma Science*, Vol. 39, No. 4, pp. 1131-1140, April 2011.

[15] H. Sheng, F. Wang, C.W. Tipton, "A fault detection and protection scheme for three-level dc-dc converters based on monitoring flying capacitor voltage", *IEEE Trans. on Power Electronics*, Vol. 27, No. 2, pp. 685-697, February 2012.

[16] J. Diaz, P.J.V.Saiz, J.A.M. Ramos, A.M. Pernia, and J. A. Martinez, "A high voltage AC/DC resonant converter based on PRC with single capacitor a output filter," *IEEE Trans. on Industry Applications*, Vol. 46, No. 6, pp. 2134-2142, December 2010.

[17] Y-C. Chuang, Y-L. Ke, H-S. Chuang and Y-M. Chen, "Analysis and implementation of half-bridge series-parallel resonant converter for battery chargers", *IEEE Trans. on Industry Applications*, Vol. 47, No. 1, pp. 258-270, February 2011.

[18] R.L. Steigerwald, "A comparison of Half-Bridge Resonant Converter Topologies", *IEEE Trans. on Power Electronics*, Vol. 3, No.2, pp. 174-182, April 1988.

[19] X. Wu, G. Hua, J. Zhang and Z. Qian, "A new current-driven synchronous rectifier for series-parallel resonant (LLC) dc-dc converter", *IEEE Trans. on Industrial Electronics*, Vol. 58, No. 1, pp. 289-297, January 2011.

[20] S.C. Wong and A.D. Brown, "Analysis, modeling and simulation of series-parallel resonant converter circuits", *IEEE Trans. on Power Electronics*, Vol. 10, No.5, pp. 605-614, Sept 1995.

[21] R. Oruganti and F.C. Lee, "Resonant Power Processors, Part II-Methods of Control", *IEEE Trans. on Industry Applications*, Vol, IA-21, No.6 , pp.1461-1471, Dec 1985.

[22] H. Chen, E.K. Sng, K-J Tseng, "Generalized optimal trajectory control for closed loop control of series-parallel resonant converter", *IEEE Trans. on Power Elecronics*, Vol. 21, No. 5, pp. 1347, Sept 2006.

[23] K. Sano and H. Fujita, "Performance of high-efficiency switched-capacitor-based resonant converter with phase-shift control", *IEEE Trans. on Power Electronics*, Vol. 26, No. 2, pp. 344-354, February 2011.

[24] M.S. Agamy and P.K. Jain, "A variable frequency phase-shift modulated three-level resonant single-stage power factor correction converter", *IEEE Trans. on Power Electronics*, Vol. 23, No. 5, pp. 2290-2300, Sept 2008.

[25] A.K.S. Bhat, "Fixed-frequency PWM series-parallel resonant converter,", *IEEE Trans. on Industry Applications*, Vol. 28, No.5, pp. 1002-1009, Sept 1992.

[26] I.Batarseh and C.Q. Lee, "High-frequency high-order parallel resonant converter," *IEEE Trans. on Industrial Electronics*, Vol. 36, No. 4, pp. 485-498, Nov. 1989.

[27] M.K. Kazimierczuk, N. Thirunaragan and S. Wang, "Analysis of series-parallel resonant converter," *IEEE Trans Aerospace Electronic Systems*, Vol. 29, No.1, pp. 278-287, Jan 1993.

[28] A.K.S. Bhat and S.B. Dewan, "Analysis and design of a high frequency resonant converter using LCC-type commutation", *IEEE Trans. Power Electronics*, Vol. 8, No. 4, pp. 291-300, July 1993.

[29] P. Jain and J.E. Quaicoe, "Modeling and analysis of fixed-frequency phase-shift modulated tertiary-side parallel-tuned resonant DC/DC converter", *IAS annual meeting* 1993, pp. 1081-1089.

[30] D. Czarkowski and M. K. Kazimierczuk, "Phase-controlled series-parallel resonant converter", *IEEE Trans. on Power Electronics*, Vol. 8, No.3, July 1993.

[31] I. Batarseh and K. Siri, "Generalized Approach to the small-signal modeling of DC-to-DC resonant converters", *IEEE Trans. on Aerospace Electronic Systems*, Vol. 29, No.3, pp. 894-909, July 1993.

[32] V. Agarwal and A. K. S. Bhat, "Small signal analysis of the LCC-type parallel resonant converter using discrete time domain modeling", *IEEE Trans. on Industrial Electronics*, Vol. 42, No. 6, pp. 604-614, Dec 1995.

[33] V. Agarwal and A. K. S. Bhat, "Dynamic analysis of the fixed-frequency PWM LCC-type parallel resonant converter using discrete time domain modeling", *PESC 1996*, pp.272-278.

[34] S. Zheng and D. Czarkowski, "Dynamics of a phase-controlled series-parallel resonant converter", *ISCAS 2002*, pp. 819-822.
[35] V. A. Caliskan, G. C. Verghese and A. M. Stankovic, "Multi-frequency averaging dc/dc converters," *IEEE Trans. on Power Electronics*, Vol. 14, No.1, pp. 124-133, Jan 1999.
[36] S.R. Sanders, J.M. Noworolski, X.Z. Liu and G.C. Verghese, "Generalised Averaging Method for Power Conversion Circuits", *IEEE Trans. on Power Electronics*, Vol. 6, No. 2, pp.251-259, April 1991.
[37] Z.M. Ye, P.K. Jain and P.C. Sen, "Modeling of High Frequency Resonant Inverter System in Phasor Domain for Fast Simulation and Control Design", *PESC 2008*, pp. 2090-2096.
[38] Z.M. Ye, P.K. Jain and P.C. Sen, "Multiple Frequency Modeling of High Frequency Resonant Inverter System", *PESC 2004*, pp. 4107-4113.
[39] V. Agarwal, V.K. Belaguli, "Large signal analysis using discrete time domain modeling for LCC-type parallel resonant converter operating in discontinuous current mode," *CCECE 1993*, pp. 80-83.
[40] V. Agarwal and A. K. S. Bhat, "Large signal analysis of the LCC-type parallel resonant converter using discrete time domain modeling", *IEEE Trans. on Power Electronics*, Vol. 10, No. 2, pp. 222-238, March 1995.
[41] J.L. Sosa, M. Castilla, J. Miret, L. Garcia de Vicuna and J. Matas, "Modeling and performance analysis of the DC/DC series-parallel resonant converter operating with discrete self-sustained phase-shift modulation technique,", *IEEE Trans. on Industrial Electronics*, Vol. 56, No. 3, pp. 697-705, March 2009.
[42] M. Castilla, L. Garcia de Vicuna, J.M.Guerrero, J. Matas and J. Miret, "Sliding-mode control of quantum series-parallel resonant converters via input-output linearization", *IEEE Trans. on Industrial Electronics*, Vol. 52, No. 2, pp. 566-575, April 2005.
[43] O. Ojo, "Robust control of series parallel resonant converters", *IEE Proceedings on control theory and applications,* Vol. 142, Issue 5, pp. 401-410, Sept 1995.
[44] R.B. Ridley, B.H. Cho and F.C. Lee, "Analysis and Interpretation of Loop Gains of Multiloop-controlled Switching Regulators," *IEEE Trans. on Power Electronics*, Vol. 3, No. 4, pp. 489-498, October 1988.
[45] A. Roshan, R. Burgos, A.C. Baisden, F. Wang and D. Boroyevich, "A D-Q Frame Controller for a Full-Bridge Single Phase Inverter Used in Small Distributed Power Generation Systems," *APEC 2007*, pp. 641-647

Ahmed A. Aboushady received the B.Eng. (Hons) and M.Sc degrees from the Arab Academy for Science and Technology (AAST), Alexandria, Egypt in 2005 and 2008 respectively. Since 2005, he has been a teaching assistant at AAST and is currently on study leave awaiting his Ph.D viva voce examination. He is expecting to be awarded his Ph.D degree in December 2012 from the electrical and electronic engineering department, Strathclyde University, Glasgow, UK. His research interests include dc/dc converters, multilevel converters, HVDC systems, power quality and advanced control systems.

Khaled H. Ahmed received the B.Sc. (first class honours) and M.Sc. degrees from the Faculty of Engineering, Alexandria University, Egypt in 2002 and 2004, respectively. He received the Ph.D. degree in electrical engineering from the Electrical Department, Strathclyde University, Glasgow, UK, 2008. Since 2009, he has been a Lecturer at the Alexandria University, Alexandria, Egypt. He has authored or coauthored more than 48 technical papers in refereed journals and conferences. Dr. Khaled is an IEEE senior member and a reviewer for the IEEE Transactions and several conferences. His research interests are digital control of power electronic systems, power quality, micro-grids, distributed generation and HVDC.

Stephen J. Finney obtained an MEng degree in Electrical and Electronic Engineering from Loughborough University of Technology in 1988. He worked for the Electricity Council Research Centre before joining the power electronics research group at Heriot-Watt University in 1990, receiving the award of PhD in 1994. From 1994 to 2005 he was a member of academic staff at Heriot-Watt University. In 2005 he moved to the University of Strathclyde where he is and currently Professor with the Institute of Energy and Environment , specialising in power electronic systems. His research interests include the power electronics for high power applications and the management of distributed energy resources. He has published extensively in IEEE and IEE journals.

Barry W. Williams received the M.Eng.Sc. degree from the University of Adelaide, Australia, in 1978, and the Ph.D. degree from Cambridge University, Cambridge, U.K., in 1980. After seven years as a Lecturer at Imperial College, University of London, U.K., he was appointed to a Chair of Electrical Engineering at Heriot-Watt University, Edinburgh, U.K, in 1986. He is currently a Professor at Strathclyde University, UK. His teaching covers power electronics (in which he has a free internet text) and drive systems. His research activities include power semiconductor modeling and protection, converter topologies, soft switching techniques, and application of ASICs and microprocessors to industrial electronics.